Chinese Journal of Chemical Engineering 90 (2026) 380–389

Contents lists available at ScienceDirect

Chinese Journal of Chemical Engineering

journal homepage: www.elsevier.com/locate/CJChE

Full Length Article

Construction of macromolecular model for Ningdong coal and simulation of gasification reaction

Longge Zhang [1], Xuelan Zhang [1], Ping Li [1,*], Yiran Zhang [1], Jiancheng Wang [2], Xingjun Wang [3]

[1] State Key Laboratory of High-efficiency Utilization of Coal and Green Chemical Engineering, College of Chemistry and Chemical Engineering, Ningxia University, Yinchuan 750021, China
[2] State Key Laboratory of Clean and Efficient Coal Utilization, Taiyuan University of Technology, Taiyuan 030024, China
[3] Key Laboratory of Coal Gasification and Energy Chemical Engineering of Ministry of Education, East China University of Science and Technology, Shanghai 200237, China

ARTICLE INFO

Article history:
Received 25 December 2024
Received in revised form
7 March 2025
Accepted 6 May 2025
Available online 26 February 2026

Keywords:
Macromolecular model of coal
Spectral simulation
Reaction molecular dynamics
Coal gasification

ABSTRACT

Understanding the structure of coal is helpful to understand the diverse reactivity of coal at a molecular scale and offer support for clean and effective utilization of coal. The physical properties of a typical coal from east of Ningxia were characterized by some analysis methods such as elemental analysis, FT-IR, XPS, and ^{13}C NMR. And the key parameters of the microstructure of the coal sample were obtained such as the type, valence and chemical bond and so on. The molecular composition of coal has been established as $C_{202}H_{153}O_{38}N_3S_2$, and a three-dimensional representation of its molecular structure was created. The molecular dynamics approach utilizing reactive force fields was employed to model the process of coal gasification. The influence of reaction force fields and temperature on coal gasification process was investigated, and the main small molecule products in different atmospheres were tracked. It was indicated that the consumption and consumption rate of raw coal and the production of primary products increased with increasing of the temperature. All carbon elements in coal were converted into fragments with less than three carbon atoms at the H_2O atmosphere and 3500 – 4000 K, and the C_1 content can reach 97.73% at 4000 K. It was proved indirectly that the gasification reaction process had been completed. In mixed atmospheres, the gasification condition closest to industrial scenarios was $500H_2O + 1500CO_2$, yielding a CO/H_2 ratio of 3.52, matching actual outcomes. Molecular dynamics simulation of gasification process based on coal macromolecules is conducive to reveal gasification reaction mechanism.

1. Introduction

A crucial approach for investigating the chemical makeup of coal at the molecular scale is through the utilization of a molecular structure model. This model serves as a tool for understanding the intricate chemical architecture of coal at a fundamental level [1]. Basic information about coal structure can be obtained using modern analysis and calculation methods [2,3]. Currently, reaction force field molecular dynamics (ReaxFF MD) is widely used in many fields to study the mechanism of coal pyrolysis and other related issues [4]. Molecular modeling based on the characterization of real coal samples provides an effective pathway to enhance understanding of coal's macromolecular structure characteristics and its reaction mechanisms [5,6]. Using molecular modeling to characterize complex chemical systems helps to explain the properties of macroscopic systems from a macroscopic perspective, providing a theoretical basis for industrial applications. Therefore, it is crucial to examine the reaction behavior of organic matter during thermal processing by analyzing it at the molecular scale.

Using molecular simulation technology to characterize coal structure aids in comprehending the progression of coal structure's evolution from a microscopic molecular perspective. This

DOIs of original article: https://doi.org/10.1016/j.cjche.2026.01.001, https://doi.org/10.1016/j.cjche.2025.05.038.
* Corresponding author.
E-mail address: liping@nxu.edu.cn (P. Li).

https://doi.org/10.1016/j.cjche.2026.01.002

technology has been proven to be one of the effective means to study coal structure [7]. Since Fuchs and others introduced the initial coal molecular model utilizing the method of chemical statistical analysis, scholars have extensively employed the construction of coal macromolecular models [8−10]. Many scientists have conducted relevant research on the mechanism of coal pyrolysis, migration of C/H/O and other elements, heating rate, and the effect of different temperatures on pyrolysis products based on the molecular models [11,12]. In the study of coal pyrolysis using molecular dynamics method, Mo *et al.* employed a suitable coal model along with molecular dynamics simulations to investigate the pyrolysis of lignite, gaining insights into product distribution [13]. Wei *et al.* [14] found that there were many kinds of debris below C_{15} in the pyrolysis process through the construction and simulation of a Zaoquan coal pyrolysis molecular model, and obtained three different formation paths by tracking the product CO_2. Huang *et al.* [15] used dibenzyl sulfide as a model compound to predict the pyrolysis process of C—S in coal by pyrolysis products. It showed that the C—S bond first broke above the energy base point and formed intermediate s radical. The relationship between C—S structure and reactivity during coal pyrolysis was identified and analyzed at the molecular level, which confirmed the general rule of free radical reaction mechanism of raw coal pyrolysis. Cui *et al.* [16] developed a three-dimensional model for the molecular characterization of anthracite by simulating the coal structure using NMR techniques and evaluating the simulation outcomes against experimental findings. The findings further underscore the capability of molecular simulation technology to provide abundant and insightful clues regarding the intricate chemical reactions involving coal. As for the study of coal gasification by molecular dynamics. Luo *et al.* [17] meticulously chose an appropriate coal model to replicate the gasification process of coal char under diverse atmospheric conditions. It was elucidated the complex reaction pathways associated with the conversion of oxygen functional groups during gasification processwere in this study, and provide valuable insights into the underlying chemical mechanisms. Zhou *et al.* [18] studied coal-water slurry/oxygen gasification using ReaxFF-MD. The lignite decomposed into small molecules and light tar radicals at 1600−2400 K. The light tar radicals further decomposed from 2400 to 4000 K, but product changes were minimal. Complete gasification occurred at 3600 K, and yielding syngas content was the highest.

Constructing a targeted molecular model based on coal characteristics and subsequently investigating its gasification reaction behavior can offer valuable insights into the relationship between specific types of coal structures and reactivity. The molecular model of Meihuajing (MHJ) coal from the Ningdong base in Ningxia was constructed in the study. ReaxFF molecular dynamics approach was employed to investigate the gasification process of coal. The coal gasification process was simulated under various atmospheric conditions, and investigated the impact of temperature and different atmospheres on the primary products of gasification from a microscopic perspective. Some statistical analysis of coal gasification products under diverse atmospheres was handled using the Amsterdam Modeling Suite (AMS) platform so as to further understand the influence of water and carbon dioxide reactions on gasification outcomes throughout the coal gasification process. This study aims to reveal the mechanism of coal gasification reaction through the reaction of macromolecular models and provide theoretical support for the clean and efficient utilization of coal.

2. Experimental

2.1. Coal sample preparation

The coal samples in the experimental originated from the MHJ mine in Ningxia. Before analysis, the coal samples underwent rigorous preparation involving grinding with a ball mill, sieving to achieve a uniform particle size of 65 μm, and subsequent acid treatment with HCl−HF−HCl to minimize mineral impurities. Tables 1 and 2 display the results from both the proximate analysis and ultimate analysis of the prepared sample, while the atomic ratios derived from normalized elemental data are detailed in Table 3. These essential data will serve as the cornerstone for constructing the coal model [19].

2.2. Characterization analysis

2.2.1. XPS

X-ray photoelectron spectroscopy (XPS) analysis was performed using the Thermo ESCALAB250XI spectrometer (Thermo Fisher Scientific). The attenuated total reflection method was employed with a resolution of 4 cm^{-1}, a spectral range extending from 600 to 4000 cm^{-1}, and 32 cumulative scans conducted. The full spectrum scan was performed at a transmission energy of 100 eV with a step size of 1 eV. Additionally, the elements C, O, N, and S were each examined using narrow scans at a transmission energy of 30 eV and a step size of 0.05 eV. A monochromatic Al K_α ($h\nu = 1486.6$ eV) source was used for excitation.

2.2.2. FT-IR

FT-IR analysis was performed using the Nicolet 380 infrared spectrometer (Thermo Fisher Scientific, USA). The attenuated total reflection method was used with a resolution of 4 cm^{-1}, a spectral range of 600−4000 cm^{-1}, and 32 cumulative scans. The KBr pellet method was used for sample preparation: the pellet was fixed on the sample holder and placed in the sample chamber for infrared spectrum analysis.

2.2.3. Solid-state ^{13}C NMR

The solid-state ^{13}C NMR spectroscopy of coal was performed using a JNM-ECZ600R600 trillion solid-state nuclear magnetic resonance instrument. MAS (magic angle spinning) and CP (cross-

Table 1
Proximate analysis results of MHJ coal.

Sample	Proximate analysis (ad)/% (mass)			
	M	A	V	FC
MHJ coal	2.84	12.94	29.66	54.56
MHJ coal after acid treatment	2.01	1.13	32.06	64.80

Table 2
Ultimate analysis results of MHJ coal.

Sample	Ultimate analysis (daf)/% (mass)				
	C	H	O①	N	S
MHJ coal	72.74	4.60	19.61	1.26	1.79

① By difference.

Table 3
Atomic ratio of coal.

Sample	H/C	O/C	N/C	S/C
MHJ coal	0.758	0.202	0.015	0.009

polarization) techniques were employed, with a contact time of 5 ms, sideband suppression, and a spectral width of 3000 Hz. Solid state NMR dual probe: 6 mm ZrO_2, rotor magic angle speed: 6 kHz, frequency: 75.43 MHz, sampling time: 0.05 s.

2.3. Model construction and validation

The initial two-dimensional (2D) and three-dimensional (3D) molecular models were generated using ChemDraw and Chem3D software. The Gaussian 16 program was used to perform a comprehensive optimization of the geometric structure along with spectral simulation based on quantum chemical calculations. Geometric structure optimization was achieved using the semi-empirical AM1 method of quantum chemistry, and the density functional theory (DFT) M06-2X/3-21G all-electron methodology. The infrared spectrum was obtained through vibration analysis on the structure optimized using AM1, while the 13C NMR spectrum was derived from the geometric configuration optimized by the M06-2X/3-21G method at the B3LYP/6-31G (d, p) level. Molecular dynamics annealing was performed using the Amsterdam Modeling Suite (AMS) software, following the NVT ensemble with the H/C/O/N/S/B force field [20].

2.4. Gasification simulation

To better simulate gasification, a model of coal's multi-molecular aggregation structure was constructed by compacting 10 individual molecules. The molecules were pressurized under NPT conditions for 200 ps at 10 MPa and 900 K, followed by a 100 ps release to obtain optimized coal molecules at 0.1 MPa and 293 K. After optimization, the density of the coal structure was adjusted to 1.12 g cm^{-3}. The subsequent simulations were performed using the AMS platform. Gasification simulations were performed in AMS software using the ReaxFF module. The coal structure was positioned at the centroid of the simulation box with periodic boundary conditions applied. The reaction system for coal gasification was constructed by placing water and carbon dioxide molecules in the box. The chemical reactions during the gasification process were simulated using the CHONSZr.ff force field parameters under the NVT ensemble, with a temperature damping of 100 fs [21]. The gasification process was carried out at temperatures of 2000, 2500, 3000, 3500, and 4000 K for 250 ps, with a time step of 0.25 fs. The simulation time step for ReaxFF MD gasification calculations was set to 0.25 fs, with a total of 1000000 steps and a total duration of 250 ps.

It is noteworthy that the simulated temperatures exceed the actual temperatures, and this approach of elevating temperatures to expedite reaction times has consistently proven effective in previous research [22].

3. Results and Discussion

3.1. Physical characterization results

3.1.1. XPS spectrum analysis

XPS enables the identification of elements and their chemical environments, such as C, O, N, and S, within coal molecules. The assignment of each characteristic peak is shown in Fig. 1,

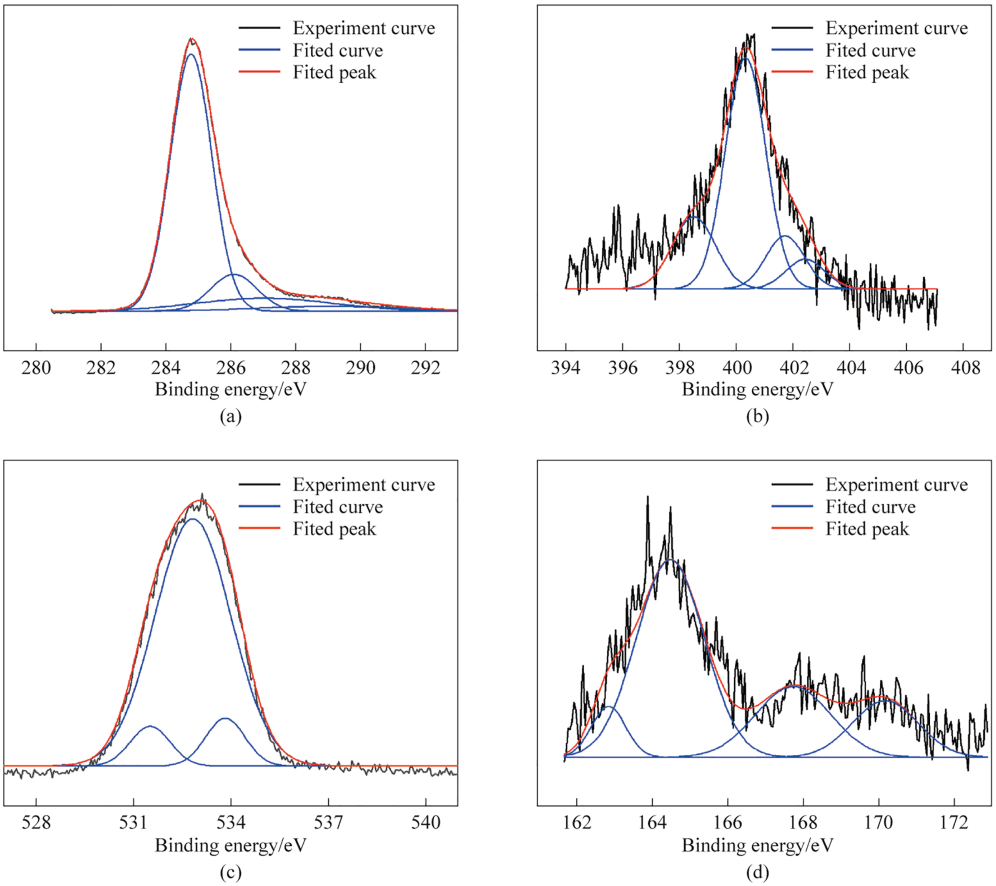

Fig. 1. Peak-fitting curves of the XPS (a) C 1s, (b) N 1s, (c) O 1s, and (d) S 2p spectrum.

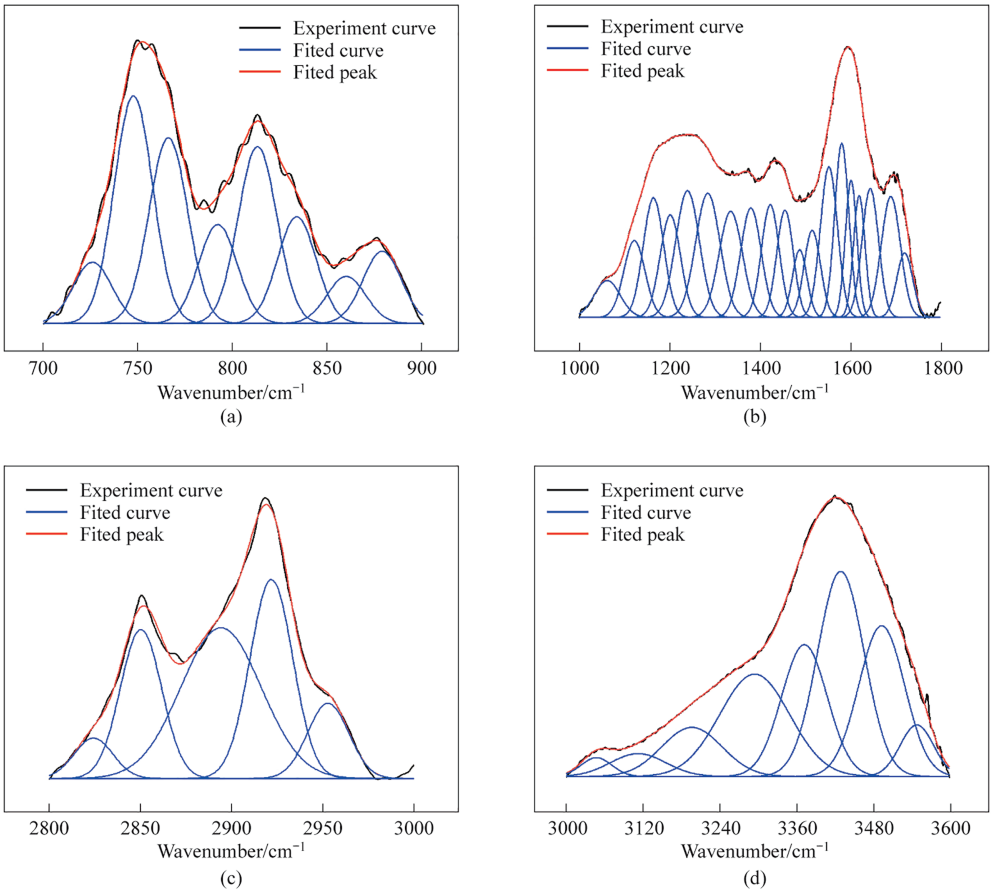

Fig. 2. Peak-fitting curves of FTIR in (a) 700–900 cm^{-1}, (b) 1000–1800 cm^{-1}, (c) 2800–3000 cm^{-1}, and (d) 3000–3600 cm^{-1}.

obtained through peak fitting of the coal XPS spectrum, and the proportion of atoms in different chemical bond environments is presented in Table 4 [23,24]. Based on the fitted peaks, it can be concluded that there are four existing forms of carbon, nitrogen, and sulfur in the coal structure, along with three distinct forms of oxygen. The XPS C 1s data presented in the table indicate that C—C/C—H bonds dominate the spectrum, comprising 71.79% of the total. Among the nitrogen functional groups identified, pyrrolic nitrogen predominated at 59.58%, followed by pyridinic nitrogen at 19.97% and quaternary nitrogen at 13.08%. The XPS O 1s spectrum revealed three distinct oxygen species, with the most prominent peak centered at 532.98 eV, corresponding to C—O functionalities. This group constituted 51.77% of the total, indicating that ether bonds (C—O—C) and hydroxyl groups (C—OH) are principal organic oxygen forms within the coal macromolecule. Furthermore, the sulfur content was primarily composed of thiophene sulfur (55.44%), sulfone sulfide (21.98%), and minor amounts of sulfonic acid, sulfate, and alkyl sulfide.

3.1.2. FT-IR spectrum analysis

Using the principles of infrared spectroscopy in conjunction with organic chemistry, the spectrum can be divided into four distinct regions, each associated with specific functional groups. The 700–900 cm^{-1} range corresponds to aromatic absorption peaks, indicating the presence of aromatic rings. The 1000–1800 cm^{-1} region primarily encompasses oxygen-containing functional groups. The aliphatic absorption band, spanning 2800–3000 cm^{-1}, indicates the presence of aliphatic chains, while the 3000–3600 cm^{-1} region corresponds to the hydroxyl absorption band, indicating the presence of hydroxyl groups, which play a crucial role in coal's reactivity and surface properties [25]. The results of the fitting process are visually presented in Fig. 2 and numerically detailed in Table 5.

In the aromatic structure region spanning 700–900 cm^{-1}, peaks at 747 cm^{-1} suggest a prevalence of ortho disubstitution on the benzene rings. Additionally, prominent peaks at 813.79 and 834.69 cm^{-1} indicate the presence of tetra-substitution, which

Table 4
Results from curve fitting and percentage calculations based on XPS.

Element	Binding energy/eV	Contribution	Content/%
C 1s	284.75	C—C C—H	71.79
	286.07	C—OH C—O—C	11.47
	287.15	C═O	11.97
	289.08	COOH	4.75
N 1s	398.52	Pyridinic nitrogen	19.97
	400.32	Pyrrole nitrogen	59.58
	401.72	Seasonal nitrogen	13.08
	402.43	Oxidized nitrogen	7.35
O 1s	530.85	Inorganic oxygen	6.22
	531.73	C═O	21.23
	532.98	C—O	51.77
S 2p	162.84	Alkyl sulfide	7.20
	164.46	Thiophenes	55.44
	167.71	Sulfone sulfide	21.98
	170.14	Sulfonic acid and sulfate	15.36

Table 5
Curve fitting results and percentage calculation from FT-IR.

Wavenumber/cm^{-1}	Center	Contribution	Content/%
700–900	747.77	Ortho disubstitution	22.13
	766.35 792.67	Ortho trisubstitution	27.68
	813.79 834.69	Ortho tetra substitution	29.05
1000–1800	1061.17–1284.29	C—O functionalities in phenol, alcohol, ether, and ester groups	35.04
	1355.22–1422.86	CH_3 symmetrical bending	19.97
	1516.34–1602.35	C=C in aromatic	22.43
	1631.21–1752.42	Conjugate C=O	16.08
2800–3000	2823.65 2849.85	—CH_3 symmetric	63.09
	2922.17	—CH_2 symmetric	27.05
	2953.50	—CH_3 asymmetric	9.86
3000–3600	3046.17	Aromatic hydrocarbon C—H	13.28
	3294.81 3372.94	Hydroxyl ether hydrogen bond	41.22
	3308.21 to −3605.75	Self associating hydroxyl	45.50

accounts for 29.05%. In the 1000–1800 cm^{-1} range, which corresponds to oxygen-containing functional groups, the peak between 1061 and 1284 cm^{-1} represents C—O functionalities in phenol, alcohol, ether, and ester groups, constituting 35.04% of the total. The region from 1516 to 1602 cm^{-1} is dominated by aromatic hydrocarbons (C=C), accounting for 22.43%, with C=O constituting the remainder. In the range from 2800 to 3000 cm^{-1}, peaks at 2823 cm^{-1} and 2849 cm^{-1}, together accounting for approximately 63.09%, indicate the dominance of naphthenic or fatty hydrocarbons containing CH_3 groups. The peak at 2953.50 cm^{-1}, comprising 9.86%, indicates asymmetric stretching vibrations of CH_3. Within the range from 3000 to 3600 cm^{-1}, the absorption band associated with hydroxyl groups extends from 3150 to 3490 cm^{-1}, reflecting stretching vibrations of C—C in benzene rings and olefins. The interval from 3308 to 3606 cm^{-1}, on the other hand, corresponds to stretching vibrations of H in phenol and primary amine groups [26].

3.1.3. ^{13}C NMR spectrum analysis

^{13}C NMR spectra provide a direct means of acquiring data on the carbon framework of coal. Peak fitting of the ^{13}C NMR spectra was performed using Peakfit v4.12 software. By quantifying the peak areas, key structural characteristics of coal were determined. The results of the ^{13}C NMR analysis are illustrated in Fig. 3 and Table 6. Wu *et al.* [27] introduced 12 crucial parameters derived from the ^{13}C NMR spectra of the coal model. This methodology serves as a predictive tool for the chemical configurations of carbon structures within coal. Therefore, 12 parameters were calculated from the ^{13}C NMR spectra and fitting results [28].

Upon analysis, the findings reveal the intricate carbon architecture of coal. Specifically, within the aromatic components, the proportion of bridgehead carbon structures (f_a^B) was 13.40%, reflecting the coal's structural characteristics. The alkylated carbon (f_a^S) and aromatic carbons bonded to hydroxyl or ether oxygen (f_a^P) accounted for 5.75% and 6.23%, respectively, indicating the presence of alkyl chains interspersed within the aromatic configurations. The degree of aromatic ring protonation, denoted by (f_a^H), was 30.01%, while the non-protonated aromatic carbon (f_a^N) and total aromatic carbon (f_a') constituted 25.38% and 55.39%, respectively, suggesting that the coal's primary structure is predominantly aromatic. Turning to aliphatic carbons, the methylene/methine content (f_{al}^H) was 12.73%, with methyl/quaternary carbons (f_{al}^*) at 3.84%, and aliphatic carbons bonded to oxygen (f_{al}^O) accounting for 14.03%, resulting in total aliphatic carbon (f_{al}) of 30.89%. Regarding functional groups, the carbonyl and carboxyl content (f_a^C) was 13.72%, indicating the presence of oxygen-bearing functionalities in the coal. Ultimately, the coal's aromatic carbon content (f_a) was 69.11%. Collectively, the results reveal the coal's carbon structures, which were then used as the basis for constructing the corresponding coal model.

The construction process was carried out using the aforementioned 12 parameters of carbon structures (as listed in Table 7). These structural parameters revealed that the proportion of aromatic carbon was 69.11%, significantly higher than the proportion of aliphatic carbon, which was 30.89%. This suggests that aromatic carbon is the predominant component in the model, while aliphatic carbon plays a crucial role in linking aromatic structural

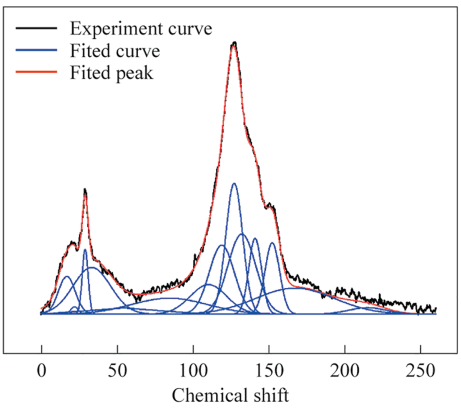

Fig. 3. Peak-fitting curves of ^{13}C NMR spectrum.

Table 6
Curve fitting results and percentage calculation from ^{13}C NMR spectrum.

Peak	Chemical shift	Ration/%	Attribution
1	17.24	3.80	R—CH_3
2	22.33	0.33	Ar—CH_3
3	29.32	2.26	CH_2
4	33.74	10.47	C,CH
5	54.27	6.79	O—CH_3, O—CH_2
6	85.04	7.24	R—O—R
7	110.86	6.48	Ar—H
8	119.64	10.37	Ar—H
9	127.83	13.16	Ar—H
10	132.91	13.4	Bridgehead (C—C)
11	141.65	5.74	Ar—C
12	152.99	6.23	Ar—O
13	168.05	12.27	COOH
14	215.85	1.45	C=O

Table 7
Percentage of structural parameters of coal sample.

	f_a	f_a^C	f'_a	f_a^N	f_a^H	f_a^P	f_a^S	f_a^B	f_{al}	f_{al}^*	f_{al}^H	f_{al}^O
Coal/%	69.11	13.72	55.39	25.38	30.01	6.23	5.75	13.40	30.89	4.13	12.73	14.03

Note: f_a—total sp^2 hybridized C; f_a^C—carbonyl or carboxyl group; f'_a —aromatic C; f_a^N —nonproonated aromatic C; f_a^H —protonated aromatic C; f_a^P —aromatic C bonded hydroxyl or ether oxygen; f_a^S —alkylated aromatic C; f_a^B —aromatic bridgehead C; f_{al}—total sp^3 hybridized C; f_{al}^*—CH_3; f_{al}^H—CH or CH_2; f_{al}^O—aliphatic C bonded oxygen.

elements. Additionally, a key parameter, XBP, represents the ratio between bridgehead and peripheral aromatic carbon. This critical parameter can be mathematically derived using Eq. (1), enabling a deeper understanding of the structural complexity and aromaticity of the molecule [29,30]. The X_{BP} value of MHJ coal was determined to be 0.319.

$$X_{BP} = \frac{f_a^B}{f_a^H + f_a^P + f_a^S} \quad (1)$$

3.2. Model construction and verification

Utilizing the findings obtained through elemental analysis, FT-IR, ^{13}C NMR, and XPS techniques, further essential parameters can be deduced for constructing the model. Initially, the identification and quantification of aromatic rings in coal molecules were determined using X_{BP} parameter, whereas the XPS and complementary characterization methods facilitated the determination of the types and counts of side-chain groups. Subsequently, the macromolecular backbone of coal molecules was structurally linked to these side-chain groups, leading to the establishment of an initial molecular model. Drawing upon the insights gained from the characterization analysis, a preliminary chemical structure sketch of MHJ coal was formulated. The primary carbon configurations were ascertained based on the ^{13}C NMR findings, with Table 8 detailing the varieties and counts of aromatic carbon structures, which encompassed two thiophenes, one pyridine, two pyrrolic, and other structures. Subsequently, the overall carbon content was validated through elemental analysis and ^{13}C NMR results. Furthermore, XPS analysis played a pivotal role in elucidating the types and abundances of aliphatic carbon. Consequently, the chemical formula for the MHJ coal model was conclusively established as $C_{202}H_{153}O_{38}N_3S_2$, with a molecular mass of 3302.72. Fig. 4 demonstrates the two-dimensional (2D) and three-dimensional (3D) structural representations of the coal.

Table 8
Types and numbers of aromatic structures in coal model.

Types	Number	Types	Number
	2	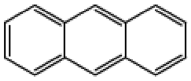	2
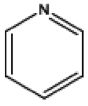	1	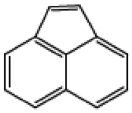	1
	2	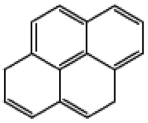	1
	1	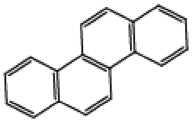	1
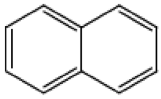	2	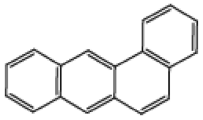	1

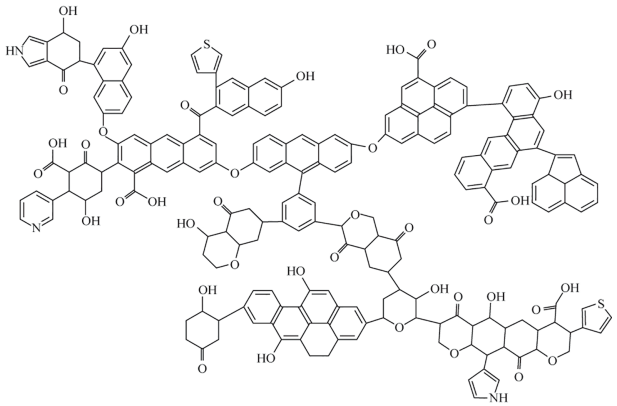

(a)

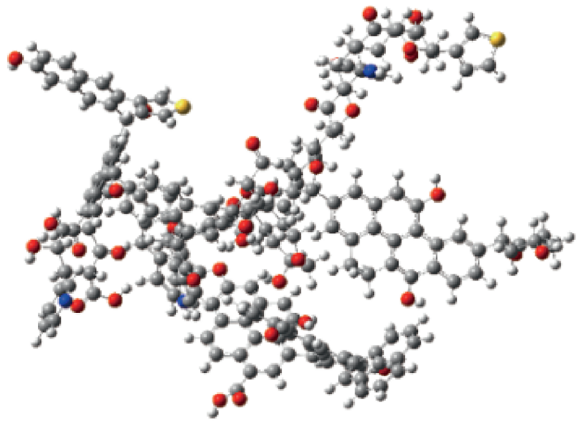

(b)

Fig. 4. Molecular model of MHJ coal: (a) 2D structure ($C_{202}H_{153}O_{38}N_3S_2$), (b) 3D optimized structure ($C_{202}H_{153}O_{38}N_3S_2$). C in gray, H in white, O in red, S in yellow, and N in blue.

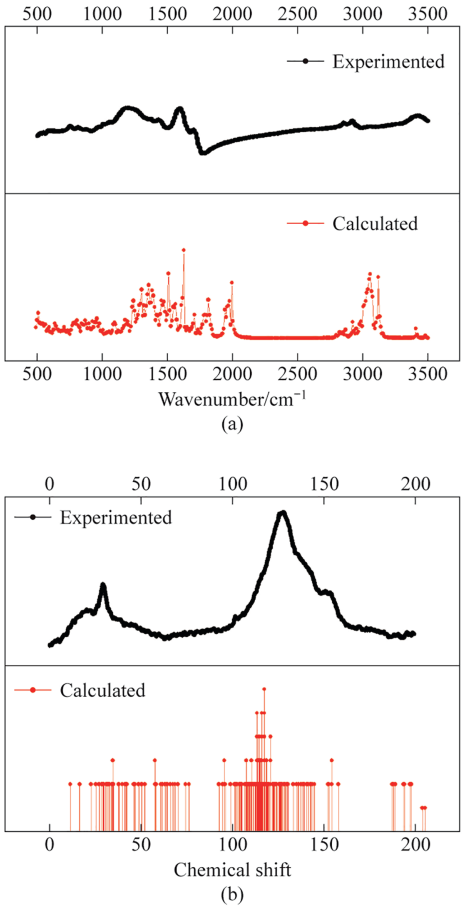

Fig. 5. Experimental and Simulated (a) IR spectrum, (b) ^{13}C NMR spectrum.

Generally, the initial model remains significantly different from the equilibrium state structure. The system's geometric configuration must be optimized to minimize its local energy. First, molecular dynamics annealing simulations were performed using AMS software to optimize the molecular conformation. Subsequently, quantum chemistry and density functional theory methods were employed to optimize the geometric structure of the dominant conformation. To validate the model's plausibility, the AM1 semi-empirical quantum chemistry method was used for vibrational analysis and infrared spectrum calculations, while solid-state nuclear magnetic resonance simulations were performed at the B3LYP/6-31G (d,p) level using density functional theory. The calculation results are presented in Fig. 5. A favorable alignment was observed between the computed FT-IR spectrum and experimental data, as well as between the simulated ^{13}C NMR spectrum and experimental findings, particularly in peak shapes and intensities. The slight discrepancies may arise from the model's reliance on the "average concept" and the inherent complexity of the coal structure [31]. The comparison of these experimental and calculated spectra further confirms rationality of the constructed coal macromolecular model.

3.3. Preparation and simulation of gasification

3.3.1. Force field selection

Given the coal structure's composition of 3980 atoms without additional atoms to facilitate reaction mechanisms, the model constructed for subsequent ReaxFF simulations is deemed reliable. Two distinct force fields, HCONSB. ff and CHONSZr.ff, were used to track the temporal evolution of primary product gases during coal gasification with H_2O and CO_2 at 3000 K.

Fig. 6(a) and (b) illustrate that under both force field conditions, H_2O consumption leads to high H_2 production and low CO_2 generation during coal gasification. However, in the CHONSZr.ff, CO levels rise as H_2O decreases, contrasting with the HCONSB. ff field where virtually no CO was formed. This is inconsistent with experimental gasification observations. As shown in Fig. 6(d), in the CO_2 atmosphere simulation, HCONSB. ff also failed to produce significant CO, while the CO_2 concentration stabilized after 50 ps. This differs from experimental findings, which show increased CO with rising CO_2 concentrations. Given the elevated simulated temperature compared to experimental conditions, initial reactions consume substantial CO_2 through C—O bond breakage, initiating CO formation [32]. Subsequently, CO_2 levels declines while CO accumulates. In CO_2 environments, elevated temperatures enhance product yields, promoting CO production during gasification, consistent with the outcomes of CHONSZr.ff. Consequently, CHONSZr.ff emerges as a superior method for describing coal gasification processes, providing more reasonable and reliable simulation results. Therefore, CHONSZr.ff will be adopted for analyzing coal gasification and product distribution under various atmospheric conditions.

3.3.2. Gasification simulation results

First, a simulation system consisting of 2000 H_2O molecules and coal aggregates was constructed. The gasification simulations were conducted for 250 ps at temperatures ranging from 2000 K to 4000 K in increments of 500 K. The study investigated the effect of temperature on coal gasification, focusing on the distribution, quantity, and types of the main gasification products.

Fig. 7 illustrates the primary changes in the number of water molecules as the temperature increases. As the temperature increases, the consumption rate of water molecules accelerates significantly. From 2000 K to 4000 K, the slope of the curve representing the number of water molecules increases with simulation time, consistent with experimental observations. At different temperatures, the final number of molecules varied with temperature. As the temperature increased, the number of water molecules decreased. At 2000 K, only 31.15% of the water molecules were consumed, whereas at 3500 K and 4000 K, the water molecule consumption rates were 87.15% and 89.20%, respectively. This indicates that the consumption rate of water molecules above 3000 K is significantly higher.

The main changes in the amounts of CO and H_2, the primary products, with increasing temperature are shown Fig. 8. The trends for both products were similar. As the temperature rised, the quantities of both CO and H_2 increased correspondingly, and higher simulated temperatures resulted in greater final amounts of CO and H_2 after 250 ps of simulation. The final quantities of CO and H_2 at 4000 K were 1191 and 2047, respectively.

Based on the statistical analysis of the types of molecular fragments after simulation at different temperatures, the products were categorized into coke (Char, C_{40+}), heavy tar (H-tar, C_{14}–C_{40}), light tar (L-tar, C_5–C_{13}), and gas (Gas, C_0–C_4) based on the number of carbon atoms.

Fig. 9 shows that as the temperature increases, the proportions of coke and heavy tar decrease significantly, while the proportion of gas increases correspondingly. The C_1–C_4 mass percentage of

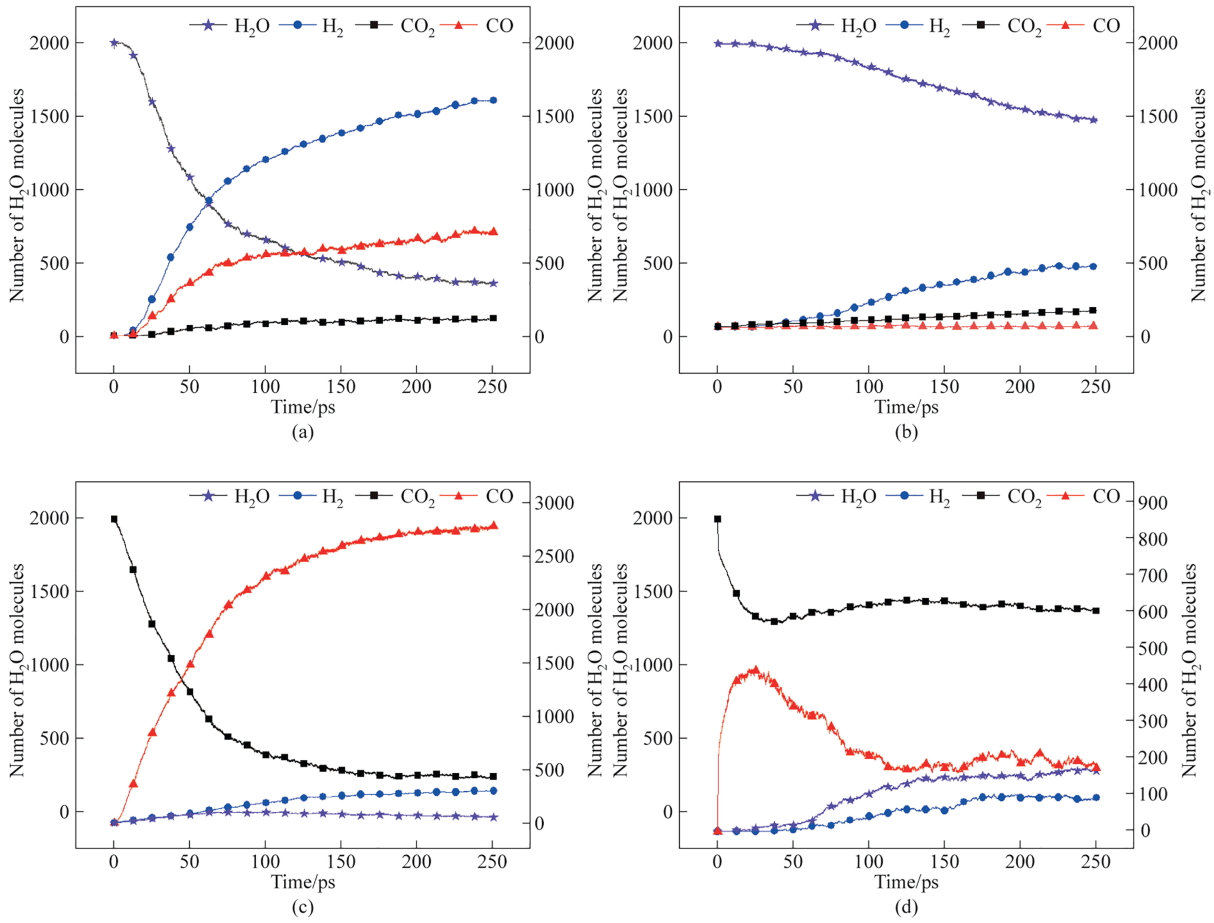

Fig. 6. Gasification simulation in the (a) H_2O atmosphere with CHONSZr.ff; (b) H_2O atmosphere with HCONSB. ff; (c) CO_2 atmosphere with CHONSZr.ff; (d) CO_2 atmosphere with HCONSB. ff.

coal after gasification simulations are listed in Table 9. Analysis of the C_1–C_4 data reveals that the C_1 concentrations at 3000, 3500, and 4000 K were 92.19%, 94.16%, and 97.73%, respectively, while no C_3 was detected at 3500 and 4000 K. These results indicated that the gasification was complete.

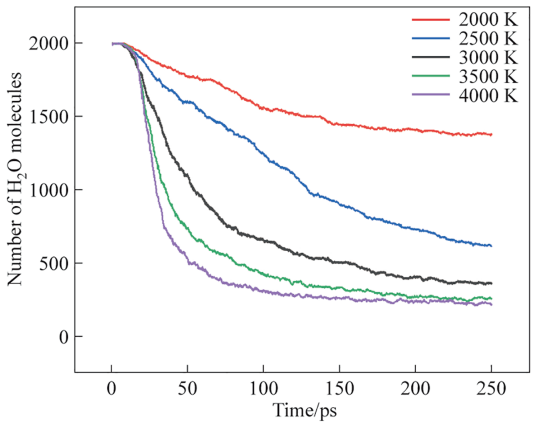

Fig. 7. Number of H_2O molecules after gasification (with H_2O) at diverse temperatures.

Based on these findings, 4000 K was selected as the simulation condition, and different reactant combinations ($1500H_2O$+$500CO_2$, $1000H_2O$+$1000CO_2$, $500H_2O$+$1500CO_2$, $2000CO_2$) were used to simulate and obtain data and parameters representative of process conditions. The initial state and final results of the gasification simulations are presented in Fig. 10 and Table 10.

Compared to the results obtained under different atmospheres, the quantities of the main products also varied with changes in the reactants at the same temperature. As the amount of carbon dioxide in the reaction atmosphere increased and the quantity of water molecules decreased, the amount of carbon monoxide in the gasification results increased, while the amount of hydrogen decreased. This indicates that increasing carbon dioxide in the gasification reaction enhances reactions related to carbon monoxide generation, and the introduction of carbon dioxide promotes the formation of carbon monoxide, as described by the related reaction $CO_2+C = 2CO$. All fundamental reactions generating carbon monoxide in the gasification process are entropy-increasing due to the generation of gas molecules [33]. The atmospheric composition of $500H_2O$+$1500CO_2$ most closely resembles the gasification conditions observed in actual industrial production. A comparative assessment of the proportions of the key gasification byproducts, CO and H_2, under varying atmospheric conditions revealed that the simulation results for the $500H_2O$ + $1500CO_2$ atmosphere exhibited the highest agreement with practical outcomes, with a CO to H_2 ratio of 3.52.

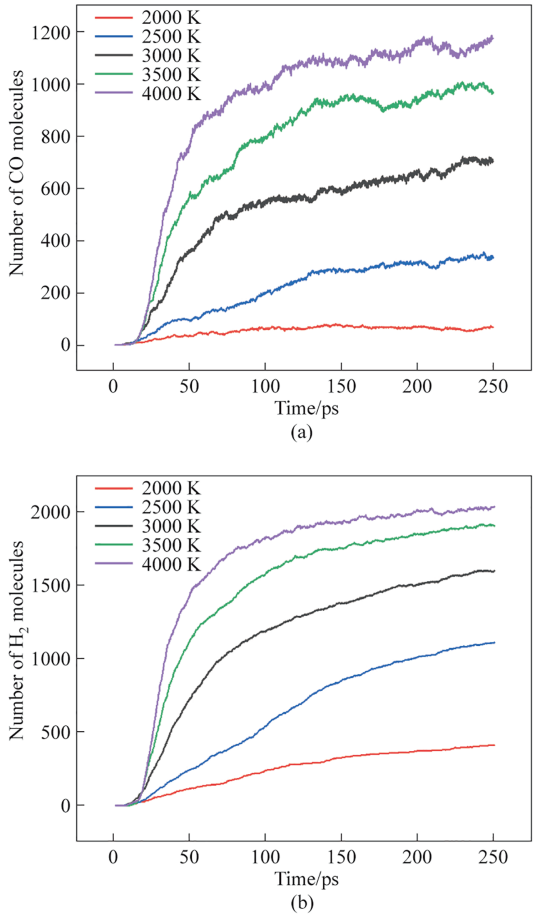

Fig. 8. Number of (a) CO molecules and (b) H_2 molecules after coal gasification (with H_2O) at different temperatures.

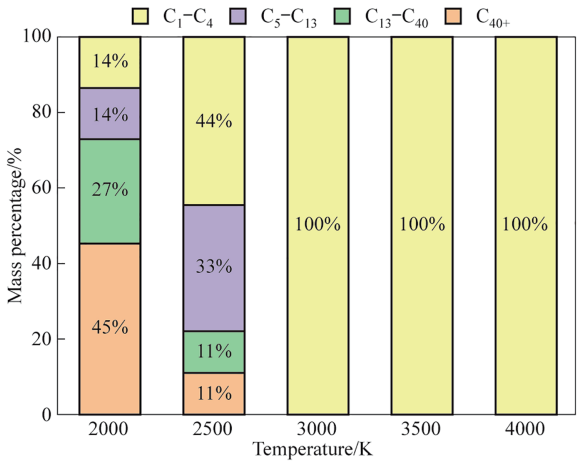

Fig. 9. Mass percentage distributions of products after coal gasification (with H_2O) at different temperatures.

Table 9
C_1–C_4 mass percentage of coal after gasification simulation.

	3000 K	3500 K	4000 K
C_1	92.19%	94.16%	97.73%
C_2	6.94%	5.84%	2.27%
C_3	0.87%	0	0
C_4	0	0	0

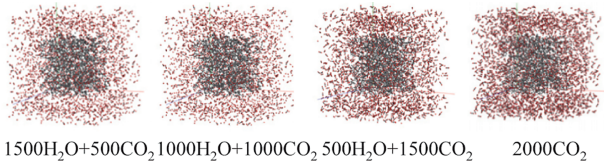

Fig. 10. Models of coal gasification reaction systems in CO_2/H_2O.

Table 10
Molecular numbers of main consumer products in different atmospheres.

Atmosphere	CO	H_2
$1500H_2O+500CO_2$	1213	1449
$1000H_2O+1000CO_2$	1705	993
$500H_2O+1500CO_2$	1840	522
$2000CO_2$	3271	397

4. Conclusions

(1) The structural model of a kind of typical gasification coal macromolecule was constructed as $C_{202}H_{153}O_{38}N_3S_2$ with a molecular weight of 3302.72, where sulfur exists as thiophene and nitrogen is present in the forms of pyrrole and pyridine. The FT-IR and 13C NMR spectra were simulated closely match experimental data, validating the coal model's accuracy in representing the complex macromolecular structure of coal.

(2) Gasification of MHJ coal in a water atmosphere was simulated. The result show that water consumption and syngas yield rose with temperature increasing. Gasification was complete when temperature arrived at 3500–4000 K. All carbon elements in the coal were converted into fragments containing fewer than three carbon atoms, with the C_1 content reaching 97.73% at 4000 K, and the macromolecular structure fragmented into small molecules like CO.

(3) A comparative analysis of coal gasification simulations under different atmospheres demonstrates that atmospheric composition significantly impacts primary gasification products. Increasing CO_2 and reducing H_2O in the mixed atmosphere enhanced CO production and reduced H_2 levels, as higher CO_2 concentrations promote CO formation via coal pyrolysis. Among the mixed atmospheres, the $500H_2O + 1500CO_2$ condition can better mimics industrial scenarios, The syngas with CO to H_2 ratio of 3.52 produced is consistent with industrial entrained flow coal gasification.

CRediT Authorship Contribution Statement

Longge Zhang: Writing – original draft, Investigation. Xuelan Zhang: Data curation. Ping Li: Writing – review & editing. Yiran Zhang: Data curation. Jiancheng Wang: Supervision. Xingjun Wang: Supervision.

Declaration of Competing Interest

The authors declare that they have no relevant financial or non-financial interests to disclose.

Acknowledgements

This work was supported by the National Natural Science Foundation of China (U21A20319) and the National Discipline Construction Project of Ningxia (NXYLXK2017A04).

References

[1] H.W. Yan, B.S. Nie, C. Peng, P.J. Liu, X.T. Wang, F.F. Yin, J. Gong, Y.Y. Wei, S.S. Lin, Molecular model construction of low-quality coal and molecular simulation of chemical bond energy combined with materials studio, *Energy Fuel.* 35 (21) (2021) 17602−17616.

[2] L.J. Li, D.M. Liu, Y.D. Cai, Y.J. Wang, Q.F. Jia, Coal structure and its implications for coalbed methane exploitation: a review, *Energy Fuel.* 35 (1) (2021) 86−110.

[3] C.Y. Wang, Y.W. Xing, K.Y. Shi, S.W. Wang, Y.C. Xia, J.H. Li, X.H. Gui, Chemical structure characteristics and model construction of coal with three kinds of coalification degrees, *ACS Omega* 9 (1) (2023) 1881−1893.

[4] T. Xu, D.K. Hong, C.B. Wang, Y. Zhang, Y.H. Li, Investigation of N migration during municipal sludge/coal co-pyrolysis *via* ReaxFF molecular dynamics, *Energy Fuel.* 37 (17) (2023) 12776−12787.

[5] X.F. Liu, D.Z. Song, X.Q. He, B.S. Nie, Q. Wang, R. Sun, D.L. Sun, Coal macromolecular structural characteristic and its influence on coalbed methane adsorption, *Fuel* 222 (2018) 687−694.

[6] M. Zheng, Y. Pan, Z. Wang, X.X. Li, L. Guo, Capturing the dynamic profiles of products in Hailaer brown coal pyrolysis with reactive molecular simulations and experiments, *Fuel* 268 (2020) 117290.

[7] P. Zou, A.Y. Yuan, B. Zhang, H.Q. Liu, K. Jin, H. Zhong, Study on pore structure and adsorption properties of coal and microscopic action mechanism of outburst, *Sci. Rep.* 15 (1) (2025) 7374.

[8] H.A.G. Chermin, D.W. van Krevelen, Chemical structure and properties of coal. XVII-A mathematical model of coal pyrolysis, *Fuel* 36 (1) (1957) 85−104.

[9] G.X. Li, F.J. Zheng, Q.F. Huang, J.J. Wang, B. Niu, Y.Y. Zhang, D.H. Long, Molecular insight into pyrolysis processes *via* reactive force field molecular dynamics: a state-of-the-art review, *J. Anal. Appl. Pyrolysis* 166 (2022) 105620.

[10] M.D. Casal, M.F. Vega, E. Diaz-Faes, C. Barriocanal, The influence of chemical structure on the kinetics of coal pyrolysis, *Int. J. Coal Geol.* 195 (2018) 415−422.

[11] M.J. Gao, X.X. Li, L. Guo, Pyrolysis simulations of Fugu coal by large-scale ReaxFF molecular dynamics, *Fuel Process. Technol.* 178 (2018) 197−205.

[12] J. Wang, Q.L. Hou, F.G. Zeng, G.J. Guo, Gas generation mechanisms of bituminous coal under shear stress based on ReaxFF molecular dynamics simulation, *Fuel* 298 (2021) 120240.

[13] M. Zheng, X.X. Li, F.G. Nie, L. Guo, Investigation of overall pyrolysis stages for Liulin bituminous coal by large-scale ReaxFF molecular dynamics, *Energy Fuel.* 31 (4) (2017) 3675−3683.

[14] W. Feng, H.F. Gao, G. Wang, L.L. Wu, J.Q. Xu, Z.M. Li, P. Li, H.C. Bai, Q.J. Guo, Molecular model and pyrolysis simulation of Zaoquan coal, *CIESC J.* 70 (4) (2019) 1522−1531.

[15] Z.B. Huang, W.J. Zhou, J.J. Wei, Study on the molecular structure model of tar-rich coal and its pyrolysis process, *J. Mol. Struct.* 1286 (2023) 135613.

[16] R.T. Cui, W.L. Xu, Y.P. Zhang, J.X. Wang, Y.Y. Qiao, Y.Y. Tian, In-depth understanding of the rapid pyrolysis free radical reaction regulation mechanism of C-S bonds in coal at the molecular level, *Fuel* 389 (2025) 134630.

[17] Q.F. Luo, Y.H. Bai, J.T. Wei, X.D. Song, P. Lv, J.F. Wang, W.G. Su, G.H. Lu, G.S. Yu, Insights into the oxygen-containing groups transformation during coal char gasification in H_2O/CO_2 atmosphere by using ReaxFF reactive force field, *J. Energy Inst.* 109 (2023) 101293.

[18] J.J. Zhou, J. Wang, S.Z. Tang, Z.C. Li, Y.Y. Xu, X. Niu, Simulations on coal water slurry gasification by molecular dynamics method with ReaxFF, *J. Mol. Model.* 30 (7) (2024) 213.

[19] J. Wang, Y.Q. He, H. Li, D. Yu W.N. Xie, H. Wei, The molecular structure of Inner Mongolia lignite utilizing XRD, solid state ^{13}C NMR, HRTEM and XPS techniques, *Fuel* 203 (2017) 764−773.

[20] B. Chen, Z.J. Diao, H.Y. Lu, Using the ReaxFF reactive force field for molecular dynamics simulations of the spontaneous combustion of lignite with the Hatcher lignite model, *Fuel* 116 (2014) 7−13.

[21] S. Dwivedi, M. Kowalik, N. Rosenbach, D.S. Alqarni, Y.K. Shin, Y. Yang, J.C. Mauro, A. Tanksale, A.L. Chaffee, A.C.T. van Duin, Atomistic mechanisms of thermal transformation in a Zr-metal organic framework, MIL-140C, *J. Phys. Chem. Lett.* 12 (1) (2021) 177−184.

[22] K.Y. Shi, J.Q. Chen, X.Q. Pang, F.J. Jiang, S.S. Hui, S.J. Zhang, H. Pang, Y.Y. Wang, D. Chen, X.B. Yang, B.Y. Li, T.Y. Pu, Average molecular structure model of shale kerogen: experimental characterization, structural reconstruction, and pyrolysis analysis, *Fuel* 355 (2024) 129474.

[23] K.J. Li, R. Khanna, J.L. Zhang, M. Barati, Z.J. Liu, T. Xu, T.J. Yang, V. Sahajwalla, Comprehensive investigation of various structural features of bituminous coals using advanced analytical techniques, *Energy Fuel.* 29 (11) (2015) 7178−7189.

[24] Y. Song, Y.M. Zhu, W. Li, Macromolecule simulation and CH_4 adsorption mechanism of coal vitrinite, *Appl. Surf. Sci.* 396 (2017) 291−302.

[25] B. Li, W. Zhang, Z.H. Xie, X.J. Chen, Y. Cui, FTIR and XRD microscopic characterisation of coal samples with different degrees of metamorphism, *J. Mol. Struct.* 1309 (2024) 138270.

[26] Y.K. Xiong, L.J. Jin, Y. Li, Y. Zhou, H.Q. Hu, Structural features and pyrolysis behaviors of extracts from microwave-assisted extraction of a low-rank coal with different solvents, *Energy Fuel.* 33 (1) (2019) 106−114.

[27] D. Wu, H. Zhang, G.Q. Hu, W.Y. Zhang, Fine characterization of the macromolecular structure of Huainan coal using XRD, FTIR, ^{13}C-CP/MAS NMR, SEM, and AFM techniques, *Molecules* 25 (11) (2020) 2661.

[28] Q.T. Zhang, G. Zhou, Y.Y. Hu, M.Y. Xing, R. Zhang, P.F. Wang, S.Y. Hu, Microwetting dynamic behavior and mechanism for coal dust based on low field NMR method: a case study, *Fuel* 297 (2021) 120702.

[29] M. Baysal, A. Yürüm, B. Yıldız, Y. Yürüm, Structure of some western Anatolia coals investigated by FTIR, Raman, ^{13}C solid state NMR spectroscopy and X-ray diffraction, *Int. J. Coal Geol.* 163 (2016) 166−176.

[30] Z.K. Li, X.Y. Wei, H.L. Yan, Z.M. Zong, Insight into the structural features of Zhaotong lignite using multiple techniques, *Fuel* 153 (2015) 176−182.

[31] Y.Y. Xu, Z.Q. Sun, X. Fan, F.Y. Ma, P.N. Kuznetsov, B. Chen, J.F. Wang, Building methodology for evaluating the effects of direct coal liquefaction using coal structure-chemical index, *Fuel* 305 (2021) 121568.

[32] Q.M. Shi, S.D. Cui, S.M. Wang, Y.C. Mi, Q. Sun, S.Q. Wang, C.Y. Shi, J.Z. Yu, Experiment study on CO_2 adsorption performance of thermal treated coal: inspiration for CO_2 storage after underground coal thermal treatment, *Energy* 254 (2022) 124392.

[33] G.Y. Li, A.Q. Li, H. Zhang, J.P. Wang, S.Y. Chen, Y.H. Liang, Theoretical study of the CO formation mechanism in the CO_2 gasification of lignite, *Fuel* 211 (2018) 353−362.